Electronic Supplementary Material (ESI) for Journal of Materials Chemistry A.
This journal is © The Royal Society of Chemistry 2015

Supporting Information

High Electrical Conductivity of Double-Walled Carbon Nanotube Fibers by Hydrogen Peroxide Treatments

Aarón Morelos-Gómez, Masatsugu Fujishige, Sofia Magdalena Vega-Díaz, Isamu Ito, Tomoyuki Fukuyo, Rodolfo Cruz-Silva, Ferdinando Tristán-López, Kazunori Fujisawa, Toshihiko Fujimori, Ryusuke Futamura, Katsumi Kaneko, Kenji Takeuchi,* Takuya Hayashi, Yoong Ahm Kim, Mauricio Terrones, Morinobu Endo,* Mildred S. Dresselhaus*
*Author(s), and Corresponding Author(s)**

Transmission electron microscopy (TEM) images exhibit that DWNT suffer breakage and removal of iron particles within carbon shells after H_2O_2 treatment **(Figure SI1)**. From the obtained TEM images the inner and outer wall diameters were obtained and their distribution is plotted in **Figure SI2**. Raman spectra for pristine and H_2O_2 treated DWNTs at 2.54 eV, 2.33 eV, 1.96 eV, 1.69 eV and 1.16 eV laser excitation energies were obtained. In Figure SI3 the D-band and G'-band are shown with small differences among them **(Figure SI3)**. Metallic and semiconducting SWNT samples were analyzed by Raman spectroscopy with 532 nm and 785 nm laser excitation wavelength **(Figure SI4 and SI5)**, in order to assess any variations due to nanotube electronic properties when treating the nanotubes with H_2O_2. X-ray diffraction patterns for pristine DWNT and DWNT-H2O2 **(Figure SI6)** reveal the decrease in iron content, observed by a decrease in the intensity of the (110) plane diffraction line of Fe. The semiquantification of the atomic composition and functionalities **(Table SI1)** reveals that the H_2O_2 oxidizes the DWNTs, introducing C-O groups. The electrical resistivity data was fitted according to the variable range hopping model $\rho(T) = \rho_0 \exp[-T_0/T]^{1/(d+1)}$ for d=1,2 and 3 **(Figure SI7)**, and the linear regression was obtained for each DWNT fiber treatment **(Table SI2)**; showing that the pristine DWNT, DWNT-Ag NP and DWNT-NH_3 are best fit for d=1 and that DWNT-I and DWNT-H_2O_2 are best fit for d=3. In **figure SI8** the DWNT fiber density and electrical resistivity are plotted against the number of twists.

SUPPORTING INFORMATION

Morelos-Gómez et al.

Table SI1 Percentage semiquantification of atomic compositions and functionalities in the pristine (DWNT) and the treated H_2O_2 treated double walled carbon nanotubes (DWNT-H_2O_2).

	DWNT	DWNT-H_2O_2
C	95.39	85.55
O	3.96	13.63
Fe	0.65	0.82
C=C	91.22	82.91
C-C	8.78	12.25
C-O	0.00	4.78

This compositional analysis was obtained according to the obtained XPS spectra.

SUPPORTING INFORMATION

Morelos-Gómez et al.

Table SI2 R^2 values obtained for each linear regression of the variable range hopping (VRH) model $\rho(T) = \rho_0 \exp[-T_0/T]^{1/(d+1)}$ for d=1,2 and 3 applied for different DWNT fiber treatments.

Sample	VRH d=1	VRH d=2	VRH d=3
DWNT	0.96691	0.92173	0.94785
DWNT -Ag NP	0.99870	0.99204	0.98645
DWNT -NH_3	0.94821	0.94486	0.93197
DWNT -I	0.99004	0.99796	0.99963
DWNT -H_2O_2	0.99518	0.99872	0.99958

SUPPORTING INFORMATION

Morelos-Gómez et al.

Figure SI1.

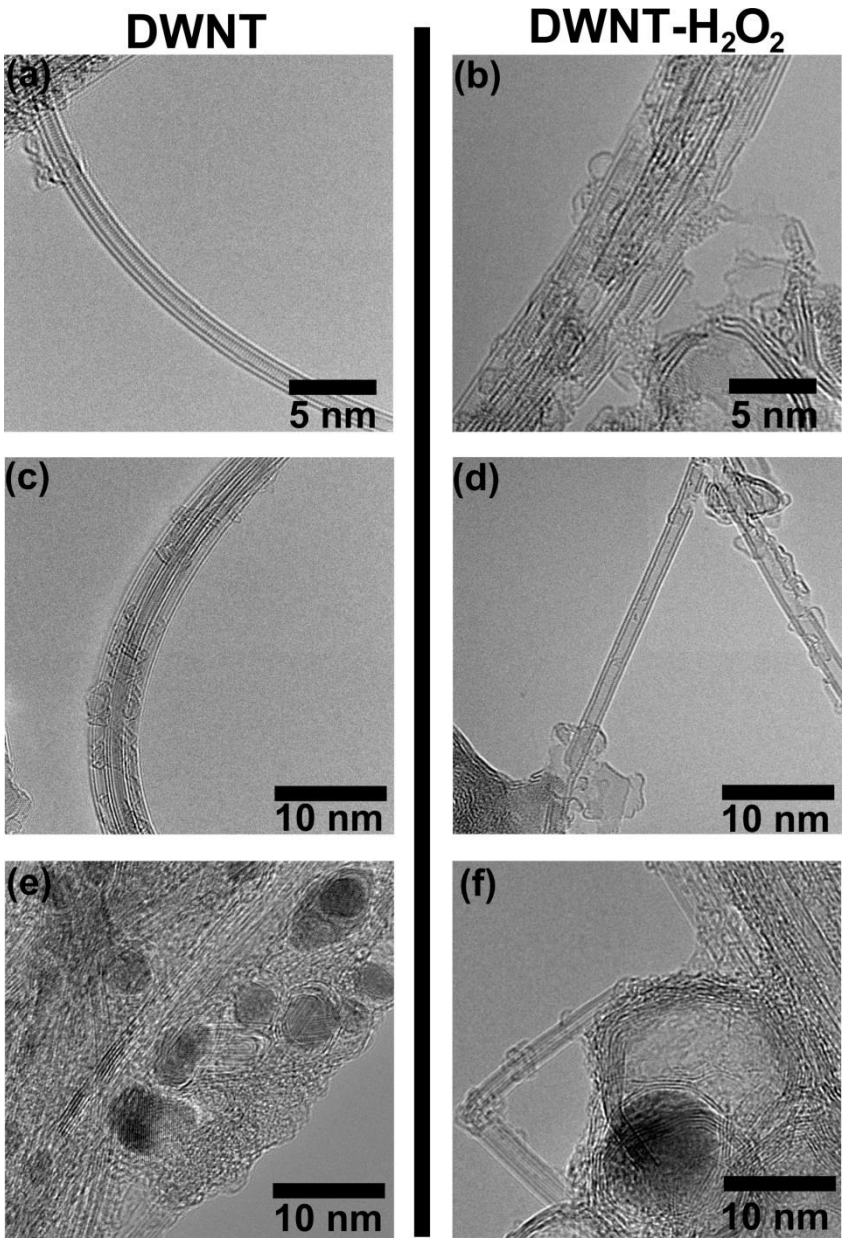

Figure SI1: Transmission electron microscopy of **(left side)** DWNT and **(right side)** corresponding DWNT-H_2O_2. The first two rows depict DWNTs structures, and show that after H_2O_2 treatment some DWNTs suffer breakage. The last row shows Fe nanoparticles, and it can be observed that, with H_2O_2 treatment, many of the nanoparticles are removed from within the carbon shell.

SUPPORTING INFORMATION

Morelos-Gómez et al.

Figure SI2.

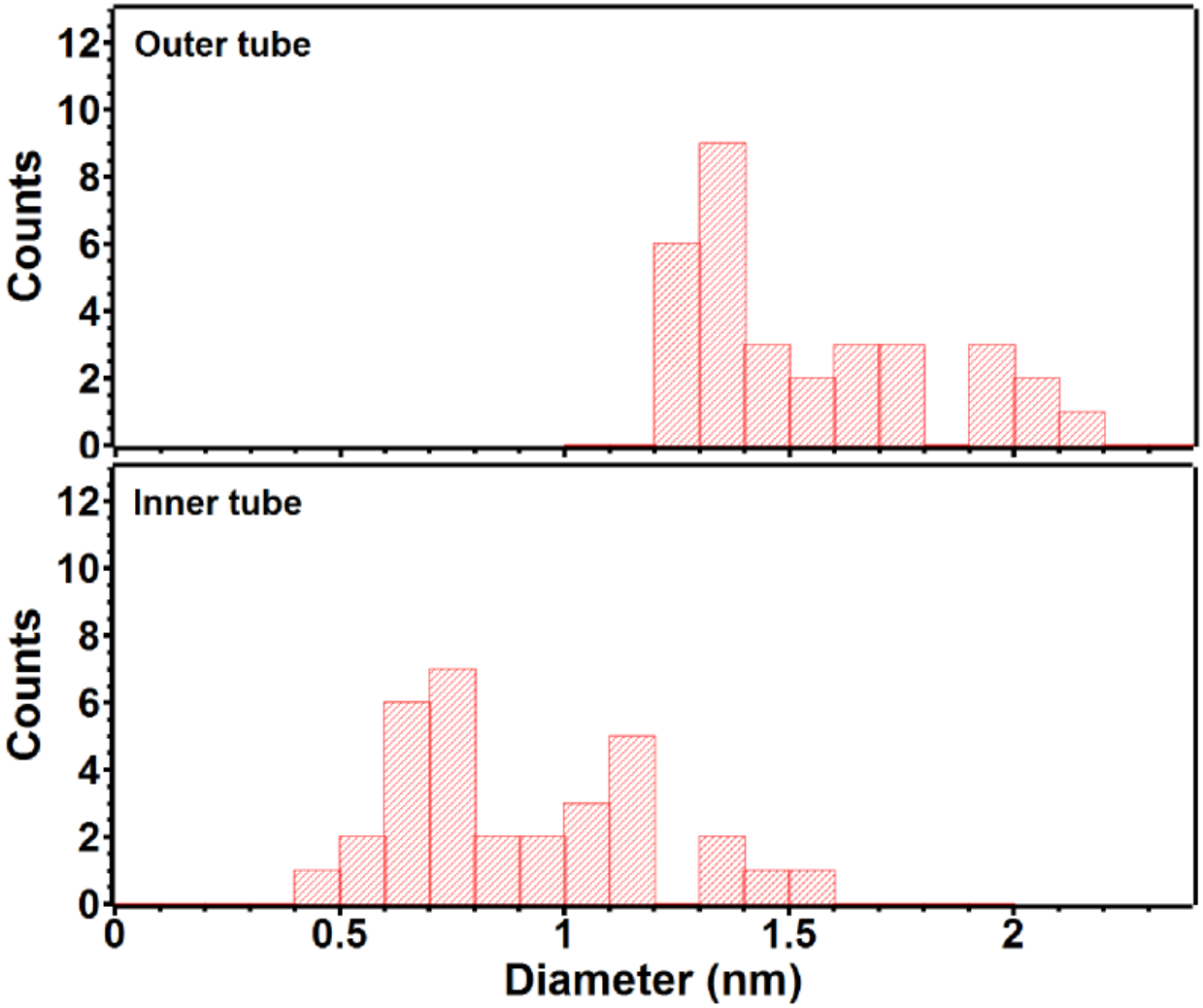

Figure SI2: Diameter distribution for the (top) outer and (bottom) inner tubes of DWNTs obtained from TEM images. The distance between the outer and inner tubes is ca. 3.35 Å.

SUPPORTING INFORMATION

Morelos-Gómez et al.

Figure SI3.

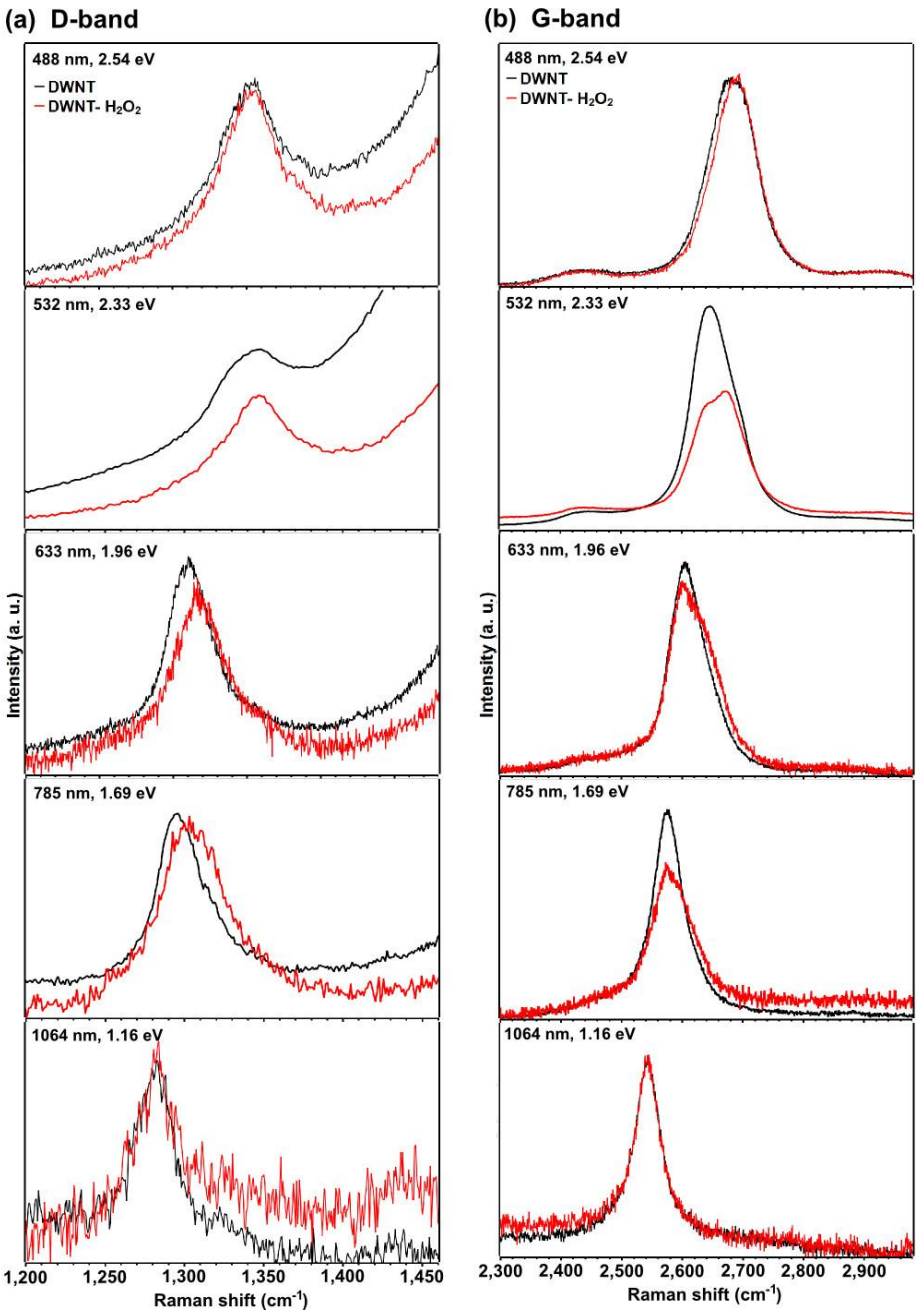

Figure SI3: Raman spectra for the **(a)** D-band and **(b)** G'-band of double walled carbon nanotubes before (DWNT) and after H_2O_2 treatment (DWNT- H_2O_2) when using 2.54 eV, 2.33 eV, 1.96 eV, 1.69 eV and 1.16 eV laser energies, also given are the corresponding laser wavelengths. All the spectra were normalized with the G-band.

In the case of M-SWNTs, the RBM peaks are upshifted, at 2.33 eV and 1.69 eV **(see Figure SI4a and b),** the D-band intensity is increased when observed at 2.33 eV **(see Figure SI3c)** and the G-band exhibits a small increase in area ca. 1558 cm^{-1} (at 2.33 eV); however at 1.69 eV (785 nm) the peak is more narrow **(see Figure SI4e and f)**, suggesting the removal of SWNTs as observed by a decrease in the RBM intensity near 160 cm^{-1}. The G'-band exhibits a slight upshift with both laser energies **(see Figure SI4g and h)**. In the case of S-SWNT, the RBM also exhibits an upshift in both laser energies. In addition, there is a decrease in intensity of the peak ca. 152 cm^{-1} which is more evident at 532 nm laser irradiation corresponding to the E_{33} transition for semiconducting nanotubes with diameters above 1.2 nm **(see Figure SI5a and b)**. The D-band exhibits an increase in intensity at both observed laser energies **(see Figure SI5c and d)**. In the G-band, there is a slight upshift along with an intensity increase below 1560 cm^{-1} for 2.33 eV and a slight increase ca. 1580 cm^{-1} for 1.69 eV **(see Figure SI5e and f)**. In the G'-band region there is a small frequency upshift **(see Figure SI5g and h)**.

SUPPORTING INFORMATION

Morelos-Gómez et al.

Figure SI4.

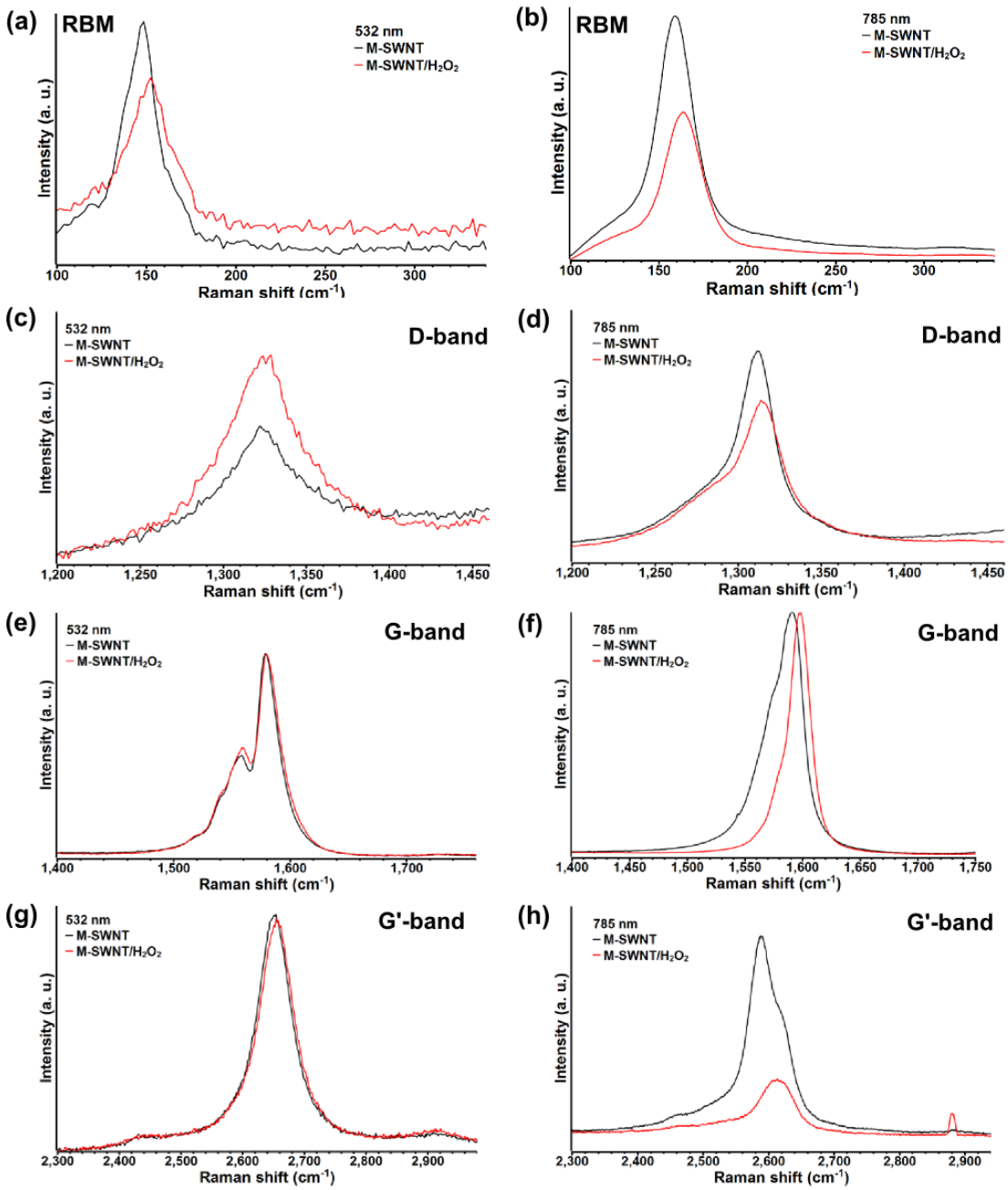

Figure SI4: Raman spectra for metallic single walled carbon nanotubes before (M-SWNT) and after (M-SWNT/ H_2O_2) H_2O_2 treatment using **(a,c,e and g)** 532 nm (2.33 eV) and **(b,d,f and h)** 785 nm (1.69 eV) laser lines. All the spectra were normalized with the G-band.

SUPPORTING INFORMATION

Morelos-Gómez et al.

Figure SI5.

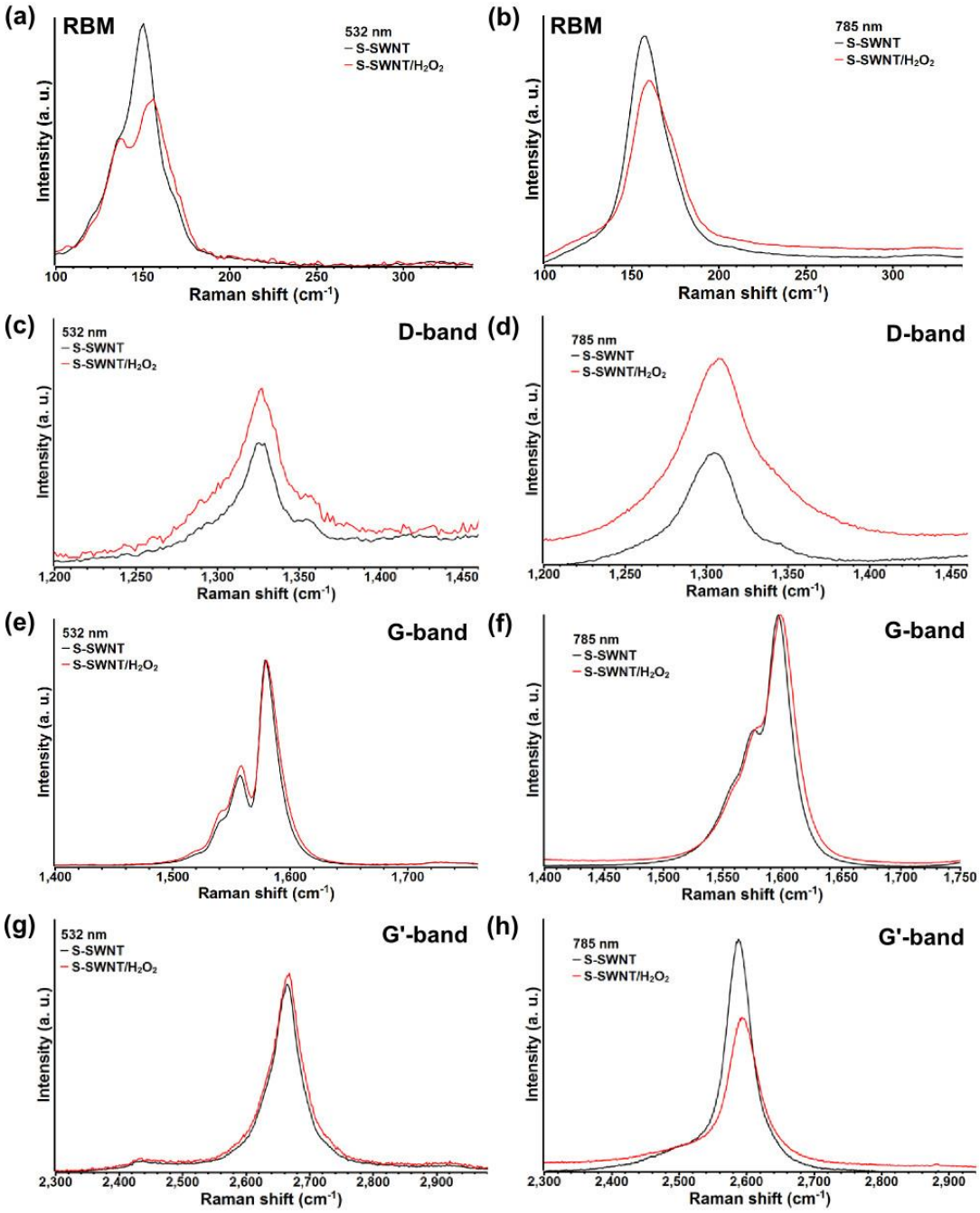

Figure SI5: Raman spectra for semiconducting single walled carbon nanotubes before (S-SWNT) and after (S-SWNT/ H_2O_2) H_2O_2 treatment using **(a,c,e and g)** 523 nm (2.33 eV) and **(b,d,f and h)** 785 nm (1.69 eV) laser lines. All the spectra were normalized with the G-band.

SUPPORTING INFORMATION

Morelos-Gómez et al.

Figure SI6.

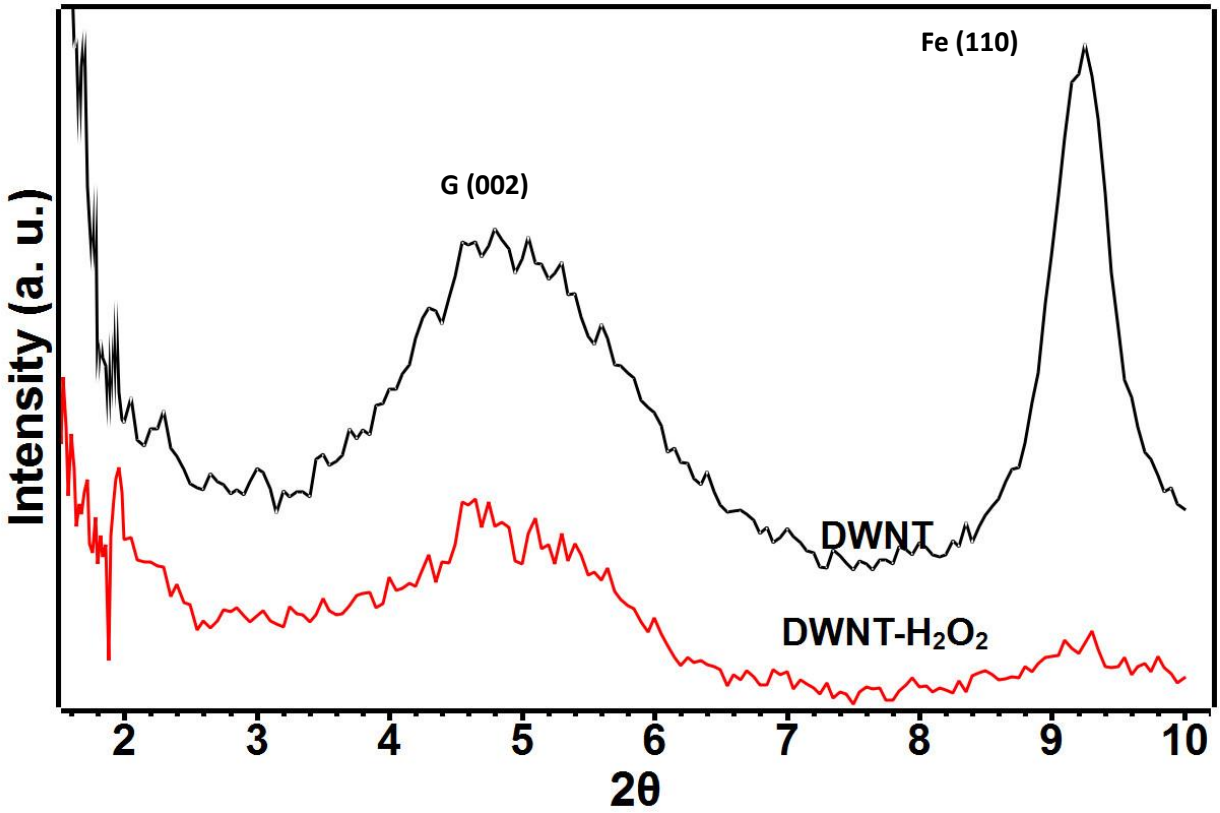

Figure SI6: Measured DWNT bundle X-ray diffraction patterns for pristine (DWNTs) and H_2O_2 treated (DWNT- H_2O_2). The peaks located at 4.9 ^{o} 2θ and 9.2 ^{o} 2θ correspond to the (002) graphitic plane of the DWNT and to the amorphous carbon, and to the (110) plane of the iron catalyst, respectively.

SUPPORTING INFORMATION

Morelos-Gómez et al.

Figure SI7.

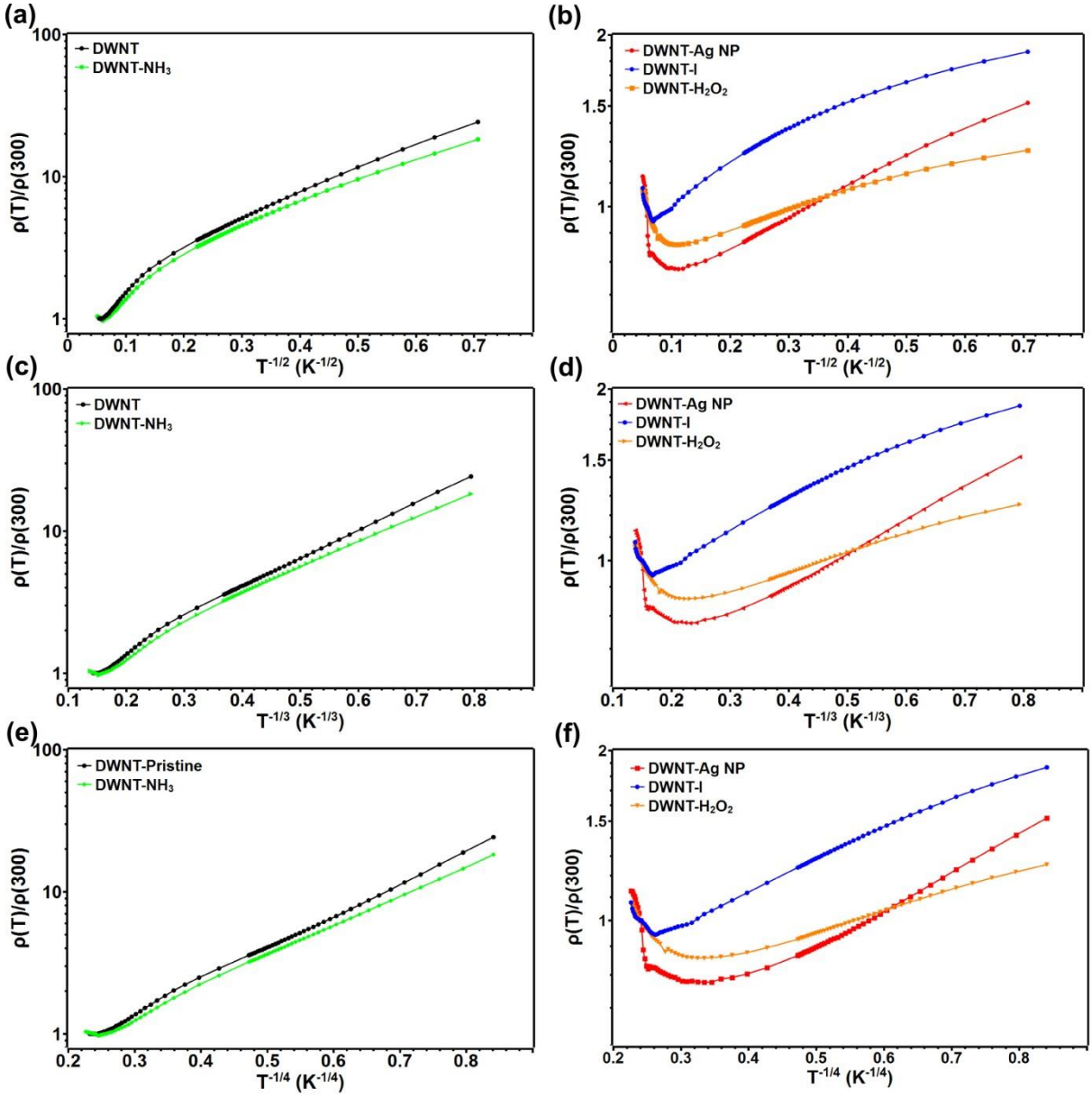

Figure SI7: Variable range hopping function fitting for **(a,b)** Coulomb gap, **(c,d)** 2-dimensional and **(e,f)** 3-dimensional models for pristine (DWNT), DWNT with silver nanoparticles (DWNT-Ag NP), DWNT soaked with NH_3 (DWNT- NH_3), DWNT with intercalated iodine (DWNT-I) and H_2O_2 treated (DWNT-H_2O_2). Dots correspond to experimental data and solid lines correspond to fittings.

SUPPORTING INFORMATION

Morelos-Gómez et al.

Figure SI8.

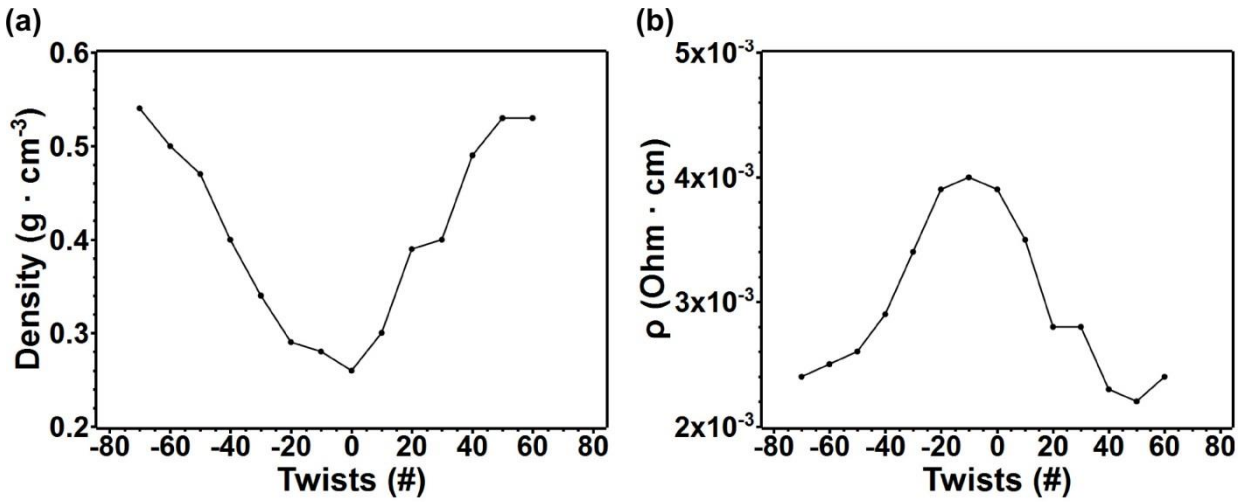

Figure SI8: The fiber was fixed at both ends and a single twist correspond to one 360° turn. Positive twists correspond to clockwise turns and negative to anti-clockwise turns. Plot of the **(a)** density vs. number of twists and the **(b)** electrical resistivity vs. number of twists. The pristine DWNT fiber was soaked in acetone and twisted, monitoring its change in density and electrical resistivity.